Available online at www.sciencedirect.com
ScienceDirect
Earth and Planetary Science Letters 251 (2006) 280–292
EPSL
www.elsevier.com/locate/epsl

The oceanic crust in 3D: Paleomagnetic reconstruction in the Troodos ophiolite gabbro

Roi Granot [a,*], Meir Abelson [b], Hagai Ron [a], Amotz Agnon [a]

[a] Institute of Earth Sciences, Hebrew University, Givat Ram, Jerusalem 91904, Israel
[b] Geological Survey of Israel, 30 Malkhey Yisrael, Jerusalem 95501, Israel

Received 28 March 2006; received in revised form 26 July 2006; accepted 5 September 2006
Available online 11 October 2006
Editor: C.P. Jaupart

Abstract

The Troodos complex, Cyprus, provides an opportunity to study the structural configuration along a fossil intersection of a spreading axis and a transform fault. We complement studies at Troodos that have reconstructed the brittle deformation of the upper crust by new paleomagnetic data from the gabbro suite. The gabbro suite is exposed at the extinct spreading axis continuing the Solea graben toward the intersection with the fossil Arakapas oceanic transform. This is a unique exposure of deep crustal rocks formed at both an inside-corner and an outside-corner of a ridge-transform intersection. Remanence directions from gabbros (23 sites) were used as indicators for rigid body rotation. The spatial distribution of rotation axes allow recognition of three regions to which deformation is partitioned: 1) a western region (outside corner) that experienced primarily tilt about horizontal axis 2) a central region with minor rotation and, 3) an eastern area (inside corner) where vertical axis rotations are dominant. The absence of significant rotation in the 6 km-wide central domain together with its location between the inside- and the outside corner uncover the root of a fossil axial volcanic zone, a zone sufficiently hot so the upper crust can decouple from the substrate. Clockwise rotation in the gabbro increases from the axial zone eastward, similar to that in the overlying dikes, indicating coupling of the lower crust with the brittle upper oceanic crust. The transition from the decoupled layers of sheeted dikes and gabbro in the axial zone to the dikes–gabbro coupling in the inside corner is in keeping with deepening of the brittle–ductile transition from the dike–gabbro boundary into the lower crust away from the axial zone. Our conclusions are consistent with one of the previous reconstructions in which the Solea spreading axis was orthogonal to the Arakapas transform fault, and with recent studies of the present-day lower oceanic crust. However, the newly inferred surface trace of the Solea spreading axis is further to the east, probably reflecting the tilt of axial upper crust rotated blocks.
© 2006 Elsevier B.V. All rights reserved.

Keywords: Troodos; ophiolite; mid-ocean ridge; lower crust; gabbro; paleomagnetism

1. Introduction

The structure of the oceanic crust influences the chemistry, biosystems, as well as the heat flow budget of the oceans. While the deformational state of the present-day upper oceanic crust is relatively known (for example see [1–4]), there are few direct observational constraints on the deformation and mechanism of spreading in the lower oceanic crust. Geophysical surveys, ocean drilling holes, and submersible means provide indications for the present-day lower oceanic crust deformation. For instance, magnetic investigations [2,5,6] and structural

* Corresponding author. Present address: Scripps Institution of Oceanography, University of California San Diego.
E-mail address: rgranot@ucsd.edu (R. Granot).

0012-821X/$ - see front matter © 2006 Elsevier B.V. All rights reserved.
doi:10.1016/j.epsl.2006.09.019

studies [7,8] of the gabbroic section have shown that the lower crust occasionally suffer significant rigid body rotation and is mostly decoupled from the upper crust. Yet, these views are either limited in their spatial coverage or provide indirect evidence for deformation. Therefore, spatial view of the deformational state of the lower oceanic crust is still poorly known.

Uplifted fragments of the oceanic crust (i.e., ophiolites) provide an opportunity to investigate the mechanism of crustal accretion within the lower oceanic crust. The lower oceanic crust in the Troodos ophiolite is represented by the gabbro suite exposed between the extinct spreading axis of the Solea graben and a fossil oceanic transform (Fig. 1). This means that the gabbro suite is exposed at a fossil ridge-transform intersection (RTI). The location of the fossil spreading axis is constrained to lie between blocks of sheeted dikes of opposite tilt [9]. In the gabbro, on the other hand, with the absence of explicit structural features, the location of the axis is more subtle. Therefore, the fossil RTI structure is obscured by the exposures of the lower crust resulting in uncertainty in the precise location of the RTI. We have designed a sampling program across the approximate location of the RTI in the lower crustal exposures. Direct observations of gabbro deformation within and near the paleo-ridge are complementary to the known deformation in the upper crust (i.e., pillow lava and sheeted dikes) and illustrate the structural evolution of the oceanic crust that takes place in a slow to intermediate spreading environment.

2. Geological setting

The Troodos ophiolite preserves a complete sequence of the ancient oceanic crust and the associated upper mantle [10] (Fig. 1). U–Pb ages of plagiogranite in the

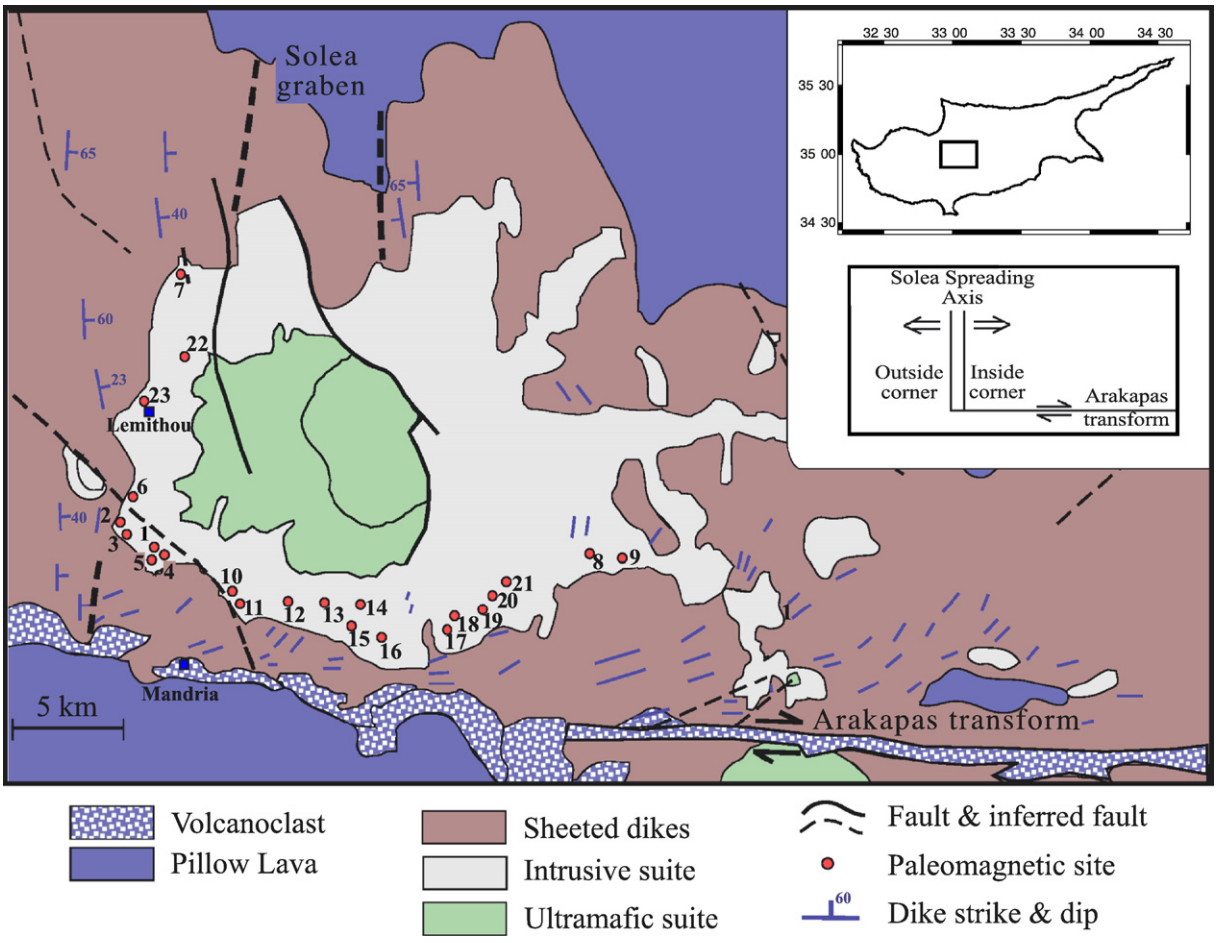

Fig. 1. Generalized geological map [44], with locations of paleomagnetic sites (red dots) in the gabbro suite. Dashed lines indicate graben axes as inferred from upper crust rotations [9]. Upper inset is a location map, and lower inset is a conceptual diagram showing main tectonic features based on the upper crust rotations [20].

Troodos sequence indicate that the ophiolite is Turonian in age, 92.1 Ma [11], suggesting formation during the Cretaceous normal magnetic Superchron spanning the period from 120.6 to 83 Ma [12]. Previous studies suggested that the Troodos massif was formed along a slow to intermediate spreading center in the suprasubduction zone within the Tethys ocean [10,13,14]. Nevertheless, the coherence of the sheeted dike complex [10], and indications that emplacement related metamorphism was minimal [15] make the Troodos ophiolite a useful analog for exploration of modern oceanic spreading centers.

Several structural features related to fossil spreading centers were identified based on structures in the sheeted dike sequence. Varga and Moores [9] identified three grabens: Solea, Mitsero and Larnaca from west to east, respectively (Fig. 1, Mitsero and Larnaca grabens are situated east and outside the geological map). It is widely accepted that the Solea graben represents a paleo-spreading axis (For example see [16]).

A zone of intense shearing elongated E–W bounds the N–S trending extensional domains in the south. This sheared zone has been ascribed to a fossil oceanic transform [9,17], henceforward named the Arakapas transform (Fig. 1). Most authors agree that the sense of motion along this transform was dextral [18,19]. Maximum deformation, with ~ 90° cumulative clockwise rotation, is evident close to the transform (i.e., sheeted dike trending E–W). The degree of rotation gradually declines with increasing distance from the Arakapas transform reaching zero 6 km to the north [20–23].

Previous studies have suggested strain partitioning between the upper crustal sheeted dikes and the gabbros of the lower Troodos crust along the spreading axis. For instance, Agar and Klitgord [24] suggested that the lower crust has undergone tilt antithetic to the upper crust, in an antithetic two-layer bookshelf-faulting model (ATLB, Fig. 2). Alternatively, Hurst et al. [14] suggested that a detachment fault separates the two parts of the crust, implying for an undeformed lower crust (Fig. 2).

2.1. The fossil ridge-transform intersection (RTI) of the Troodos ophiolite

At a RTI, an inside corner (IC) is formed between the ridge axis and the transform fault, and an outside corner (OC) is constructed on the other side of the ridge axis. The complete structure of the Troodos RTI is obscured in the plutonic complex of the lower crust and upper mantle (Fig. 1) in which structural markers are much more subtle than, for example, dike trends in the upper crust. In order to extrapolate the Solea axis towards the Arakapas transform, Macleod et al. [20] and Allerton and Vine [21] examined the sheeted dikes south of the plutonic complex, in the vicinity of the Arakapas transform. MacLeod et al. [20] have found a sharp transition between domains of steeply dipping N–S trending dikes (i.e., location of OC, Fig. 1) and domains of clockwise rotating dikes (i.e., location of IC, Fig. 1). They interpreted this transition as the location of the intersection between the Arakapas transform and the Solea spreading axis. Accordingly, the RTI is orthogonal under this interpretation. Still, the linkage between the Solea axis and the location of the fossil RTI suggested by Macleod et al. [20] is not clear, especially considering the curving planform of the Solea graben as mapped by Abelson et al. [25]. The curving axis would imply a curved, rather than rectangular RTI as suggested by Macleod et al. [20].

In the present study we re-examine the shape and location of the Solea fossil axis in the gabbro suite. We use paleomagnetic tools in order to reconstruct the spreading related rotations. The location of the fossil axis in the lower crust can be identified by the OC and IC deformation in the gabbro, reconstructed independently by paleomagnetic measurements. We further define the locus of the root of the axial-volcanic-zone in the lower crust by the absence of rotation in the gabbro suite, where the original paleomagnetic vector is preserved.

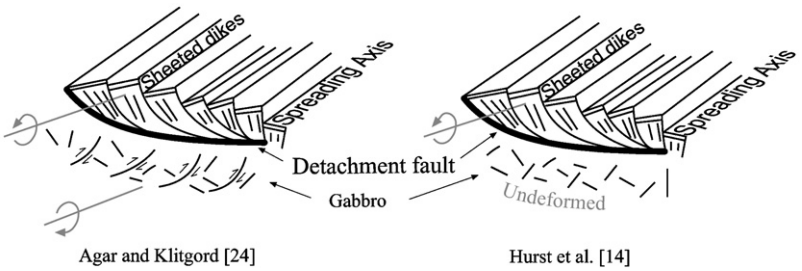

Fig. 2. Two-dimensional structural models for spreading at Troodos where the sheeted dikes are decoupled from the lower crustal gabbro. (a) Antithetic tilting of axial crust [24]. (b) Structural model where the upper crust detachated from the lower crust [14].

2.2. Previous paleomagnetic studies

Several paleomagnetic surveys conducted in Troodos have investigated the magnetization of the upper pillow lavas (e.g., [19,26]) as well as the magnetization of the sheeted dike complex (e.g., [21,22,27,28]). The entire complex had rotated by nearly 90° anti-clockwise during the late Cretaceous–early Eocene interval and recent uplift of the Troodos massif resulted in radial tilts about Mt. Olympus of 10°–20° [29]. The direction for the Troodos ophiolite mean magnetization vector (TMV) was defined as 274/36° (α_{95}=12.3°) [26]. We use the TMV as a reference for paleomagnetic reconstruction in this study.

Previous paleomagnetic and rock magnetic studies of Troodos lower oceanic crust indicate unaltered and intact gabbros [25,30]. These studies show that the characteristic remanent magnetization (ChRM) is primary and reside in magnetite. In addition, studies of the Oman ophiolite [31] and of the present-day oceanic crust (for example see [32–34]) have shown that the primary magnetic carrier is mostly low Ti-magnetite that acquired its magnetization during the initial intrusion time. According to their interpretation, the high temperature component of magnetization can be used to reconstruct the rigid body rotations of the lower crust. For instance, Kelemen et al. [6] have used the gabbro magnetization as a tool to reconstruct the post-accretion rigid body rotations of the lower crust at the Mid-Atlantic Ridge, near the Fifteen Twenty Fracture Zone.

3. Methods

3.1. Paleomagnetism

In order to resolve the temporal variations in the lower crust deformation, and to identify the spreading axis location (i.e., location of axial-volcanic-zone), we sampled the gabbro along two transects: 1) a flow-line as near as possible to the Arakapas transform, and 2) an approximate isochron west of the Solea axis (Fig. 1). The difference between the magnetization and the

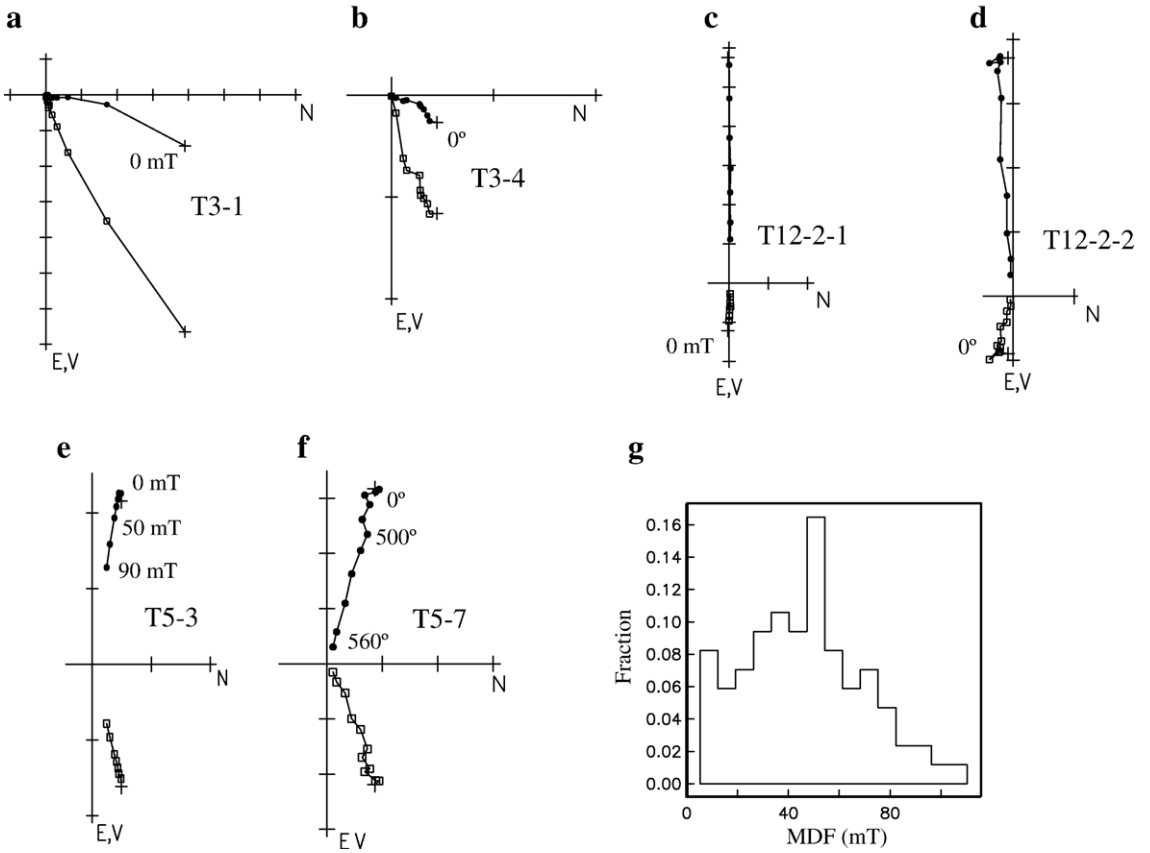

Fig. 3. a–f) Representative orthogonal vector projection of AF and thermal demagnetization experiments. Open (solid) symbols are plotted on vertical (horizontal) oriented planes. Sample ID denoted next to each plot. g) A histogram showing the median destructive field (MDF) spectrum of Gabbro samples. Samples shown in panels a–b have low MDF; panels c–d — high MDF; panels e–f — extremely high MDF.

expected TMV allows an estimate of the finite rotation that occurred between the acquisitions of the magnetization in the rocks up to the cessation of the local spreading related deformation.

We collected a total of 227 field-drilled cores oriented with a sun compass. In this study we present the results of 131 samples from the two transects. Further magnetic fabric and paleomagnetic analyses of the additional samples, located in a different spreading environment, are intended to link the lower crust magma flow patterns and the structure of the oceanic crust (unpublished data). The samples presented here were collected in 23 sites (five to seven cores of gabbro per site).

All sites were located in the upper kilometer of the lower crust. Sampling was chosen for localities that exposed structure of massive gabbros (i.e., absent of layered gabbros), and did not suffer alteration. The composition of the sampled gabbros varied between pyroxene-gabbro, olivine-gabbro, melagabbro, and uralite gabbro (for a detailed petrology description of the lower Troodos crust please see ([35]). If any, serpentinization and hydrothermal alteration of the sampled gabbros were minimal. Since low temperature alteration could not be excluded, we bound ourselves to use only data points above 200 °C.

Natural remanent magnetization (NRM) was measured in the paleomagnetic laboratory of the Institute of Earth Sciences, Hebrew University, using three axes 2G 755R SRM cryogenic magnetometer. All specimens were progressively demagnetized either by alternating field (AF) or thermal demagnetization.

For each site, two pilot specimens were first demagnetized with either demagnetization method. AF demagnetization was performed by exposing the specimen to a series of steps with increasing AF peak values. After each step the remaining remanence was measured. From each site 4 to 5 specimens were stepwise demagnetized by alternating field from 10 to 90–100 milli-Tesla (mT) in steps of 10 to 20 mT. The AF strength needed to reduce the initial remanence to half its value, called the median destructive field (MDF), gives a rough estimate of the coercivity. Two, usually companion specimens from the same AF demagnetized samples were thermally demagnetized in a step wise fashion from 100 °C to 600 °C in steps of 100 °C in the low temperature intervals to 25 °C in the high temperature intervals.

Best-fit lines to the progressive demagnetization vectors were calculated using principal component analysis [36]. We used only specimens with a maximum angle of deviation (MAD) about the principal component direction of less than 5°. The directions of the ChRM within the sites and the mean magnetization vector for each site (SMV) were calculated according to Fisher statistics [37]. Our magnetic records were divided into three structural domains. Each domain extends several

Table 1
Gabbro sites locations, site mean vectors (SMV), and their average median destructive field (MDF)

Site	N/N_0	Latitude	Longtitude	D	I	α_{95}	κ	MDF
T-1	4/6	34°53.72	32°50.34	287.1	26.1	5.5	205.9	52.4
T-2	4/6	34°54.21	32°48.85	240.1	57.6	6.5	146.5	29.7
T-3	6/6	34°53.99	32°48.99	30.6	75.3	11	31.5	10.5
T-4	5/6	34°53.64	32°49.89	275.6	28.1	10.4	43.9	15.7
T-5	5/5	34°53.76	32°50.23	282	28.4	4.6	291.7	87
T-6	7/7	34°55.45	32°49.05	342.9	81.3	4.1	185.2	80
T-7	5/5	34°59.35	32°49.90	300	71.8	8.2	69.7	33
T-8	6/6	34°54.16	32°59.16	291.4	18	3.6	278.6	49.5
T-9	6/6	34°54.05	32°59.59	319.2	13.5	5.3	133.5	40.2
T-10	5/5	34°53.07	32°52.47	295.4	22.7	3.4	390	96.5
T-11	6/6	34°53.42	32°52.10	254.5	22	4.4	194.1	67.7
T-12	6/6	34°53.42	32°52.88	272.3	12.9	4	231.6	48
T-13	6/6	34°53.47	34°53.47	254.5	− 14.7	10.5	34.3	70.5
T-14	5/5	34°53.59	32°53.94	250.3	− 8.3	3.8	313.5	53
T-15	5/5	34°52.91	32°53.93	299.7	4.6	5.3	162.2	35.6
T-16	6/6	34°52.79	32°54.38	310	− 9.1	3.6	279.3	54.7
T-17	5/5	34°53.33	32°55.96	312.8	6.7	10.5	42.6	38.7
T-18	5/5	34°53.49	32°56.13	307.5	16.9	2.1	1027.8	16.7
T-19	6/6	34°53.01	32°56.78	316.6	26.7	4.9	152.8	32.5
T-20	6/6	34°53.18	32°57.26	306.7	27.7	7.6	64.9	26.2
T-21	5/5	34°53.62	32°57.63	293.6	2.3	3.6	355.4	42
T-22	6/7	34°58.34	32°49.62	355.9	84	6.8	80.2	10.5
T-23	5/5	34°57.04	32°48.58	183	80.9	6.8	101.7	70

Statistics were calculated using the PaleoMag [46].

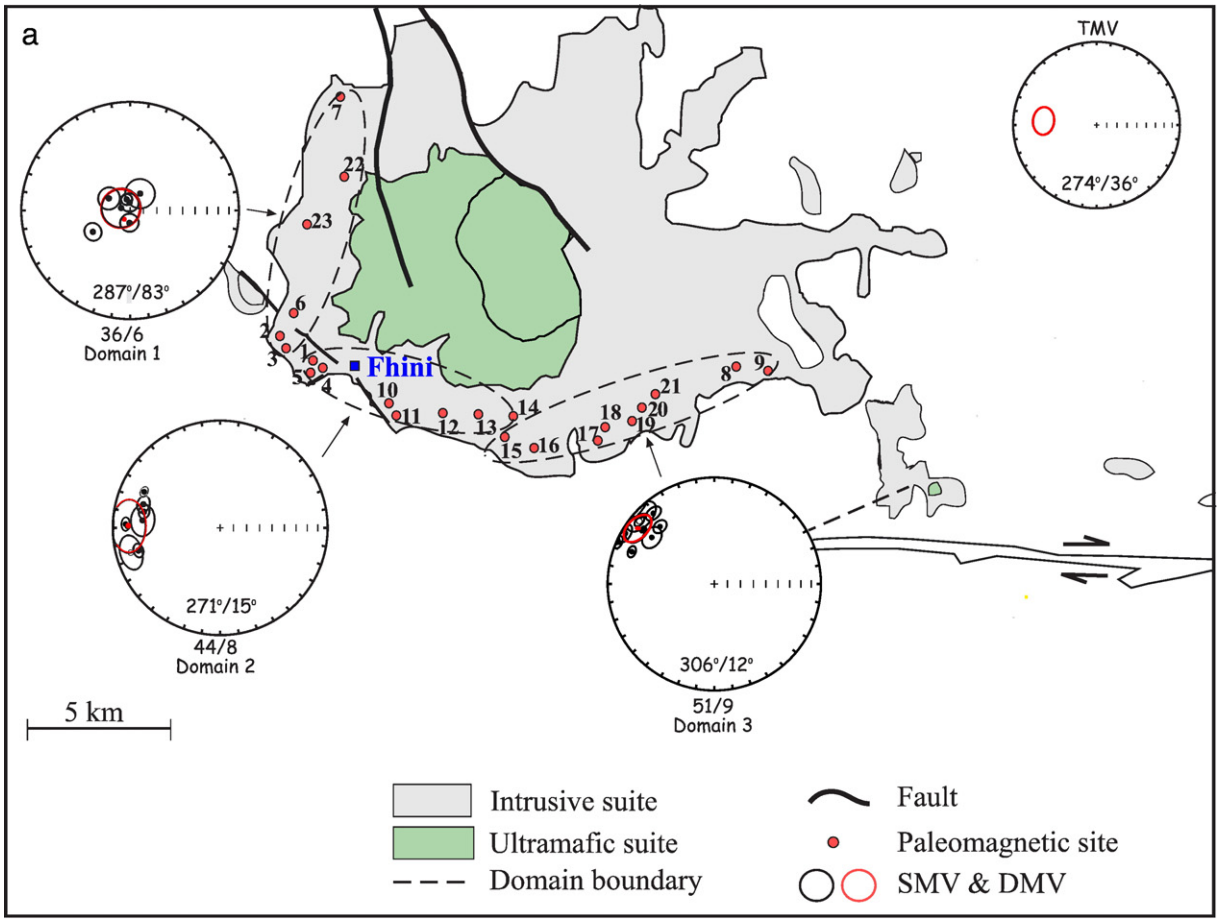

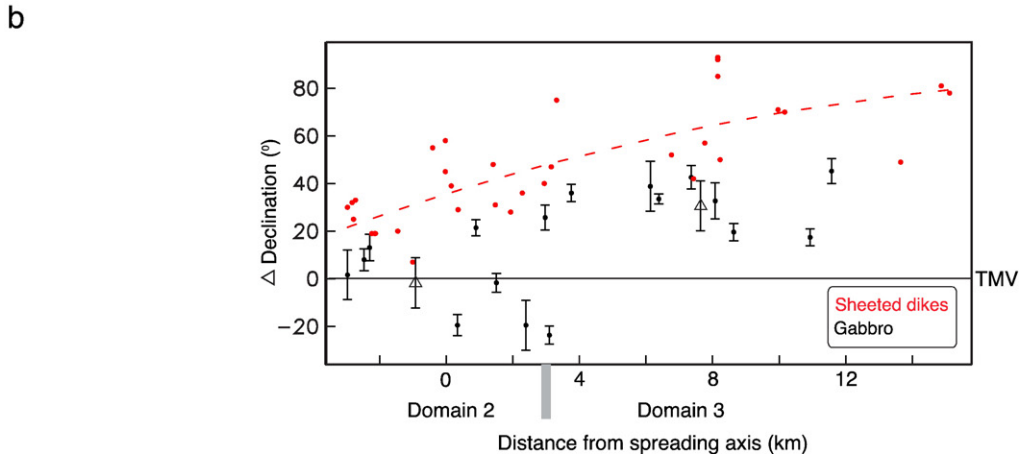

Fig. 4. Summary of paleomagnetic results. (a) Projection of SMVs and DMVs on the geological map. Below each projection are the number of specimens/number of sites in each domain. Reference magnetization direction, TMV, is shown on the upper right corner. (b) Mean declination difference from TMV of all gabbro sites (black dots) and domains (black triangles). Error bars correspond to α_{95} for each subset. Data shown for the dikes (red dots) are the deflections from the original N–S orientation of Solea axis determined from the geological map [44], averaged over width of each group of dikes. Dashed envelope represents the shear strain according to a linear strain accumulation. Rotation increases with the distance from spreading axis. Dispersions in paleomagnetic vectors are typical for the Troodos gabbro [25].

kilometers parallel to the spreading direction, therefore their magnetization represent the averaged magnetic directions over tens to hundreds of thousands of years. These directions are thought to average the magnetic paleosecular variations and therefore can be used for comparison with the TMV direction.

3.2. Structural reconstruction

The structural analysis of massive gabbro requires a conceptual model, in addition to the paleomagnetic vectors, for constraining rigid body rotation. In contrast to layered rocks and originally vertical bodies (e.g. dike and veins), massive gabbros lack information on paleo-horizons, and the paleomagnetic vectors only partially constrain the rotation. Following Abelson et al., 2002 [25] we constrain the axis of rotation sought by assuming that its trend parallels the axial graben. The plunge of the axis is then determined together with the amount of rotation. An independent test to the resulting rotations can be given by the coherence of the flow pattern as determined from fabrics [25].

4. Results

AF demagnetization reveals one or two components of magnetization. The characteristic component was isolated within 30–90 mT (Fig. 3). MDF values are mostly between 35 and 55 mT with 10% of the specimens displaying higher/lower coercivity values (Fig. 3). Thermal demagnetization reveals at most two stable components of magnetization: an occasional low temperature component (0–150 °C), and a medium to high temperature component (300–580 °C) directed toward the origin. Maximum blocking temperature of ~ 580 °C suggests that the magnetic carrier is nearly a pure magnetite (i.e., very low Ti concentration, Fig. 3). Both AF and thermal cleaning methods reveal consistent remanence directions within the cores and sites (Fig. 3). High coercivity, high unblocking temperatures, and the absence of significant alteration suggest that the remanence of magnetization is carried by relatively fine grains (pseudo to single domain) of exsolved low-Ti to pure magnetite (i.e., magnetization acquired at the time of origination).

From our results, it appears that the SMVs directions do not cluster near the mean westerly direction expected for the Troodos ophiolite (Table 1). We delineated our study area into three structural domains by comparison of the SMVs directions (Fig. 4a). Site means within each domain are averaged to give domain mean magnetic vectors (DMV). The western part, Domain 1, displays steeply inclined vectors suggesting rotation about horizontal axis. The geographical boundary of Domain 2 was set such that the 95% probability confidence cone was similar to the TMV direction. The eastern part, Domain 3, reveals relatively shallow inclinations to the NW. This suggests clockwise rotation about a steep axis. The sheeted dikes adjacent to the plutonic complex from the south display a similar trend of rotation as the lower crust. These dikes also reveal a consistent larger degree of rotation relative to the gabbro rotation (Fig. 4b).

5. Discussion

5.1. Application of gabbro paleomagnetism to the reconstruction of axial deformation

We use the mean primary ChRM and the TMV to reconstruct the rotation and by inference, the rigid body rotation history of the lower Troodos crust. Because brittle deformation occurs under the unblocking temperature of the rocks (e.g., [38,39]), the direction of magnetization present most, if not all, of the rigid body rotation history of the lower oceanic crust and can be used for structural reconstruction.

The paleomagnetic vectors provide a constraint on the finite rotation that the rock has undergone since formation. In the absence of an independent vector (such as the paleo-vertical for strata or a paleo-horizontal for dikes) the reconstruction is non unique, but using reasonable assumptions on the tectonic setting we can test various models. We set the tilt axes to align with the strike of the ancient spreading axis. The plunge of tilt axes and the amount of rotation for each domain is estimated by bringing the corresponding DMV to the TMV (Table 2). We did not rectify the data with respect to the youngest uplift and arching of Troodos as our study area lies close to the axis of this structure. Furthermore, a previous paleomagnetic study from the Troodos gabbro away from the Arakapas transform indicates average TMV direction for 8 arbitrary sampling sites [25], suggesting no differential deformation within the gabbro due to the late doming.

Table 2
Domain mean magnetic vectors (DMV) and tilt parameters

Domain	N	D	I	α_{95}	κ	Tilt axis		Rotation
						D	I	
1	6	286.6	83.1	14.6	22	0	4	47
2	8	271	15.3	16.4	12.2	180	7	21
3	9	306.3	12.1	9.8	28.4	0	53	−44

5.2. The inferred RTI deformation in the gabbro suite and the location of the extinct spreading axis

Off-axis abyssal hills from the East Pacific Rise, located near an active RTI, reveal J-shaped structures in the inside corners (Fig. 5) [3]. In these structures, the abyssal hills are deflected 15–20° from the regional trend close to the transform faults, where the shear forces are dominant. The rotation of the crest of the hills decreases to zero and they aligned with the regional trend far (20 km) from the transform faults. Therefore, rotations about a vertical axis near the Arakapas transform indicate an IC location [20,23]. Steep faults dipping toward the ridge axis with back-tilted rotation of blocks within the upper crust were observed at the Atlantic ridge outside corner [40]. Therefore, rotations about a horizontal axis near the Solea graben indicate an OC location [20,23].

We cast our paleomagnetic results in a scheme that mimics the structures inferred for active ridge-transform intersections. The lower Troodos crust reveals three different structural domains. The western part, Domain 1, has undergone rotation about a southward pointing horizontal axis with a westward tilt suggesting an OC terrain (Fig. 4a). East of Domain 1, Domain 3 has mainly undergone rotation about a vertical axis in a clockwise sense (Fig. 4). Therefore, Domain 3 is an IC terrain. These two domains resemble the deformation style found in the sheeted dikes of the upper RTI crust [20,23]. The major difference between the upper and the lower crust is found in Domain 2.

The DMV of Domain 2 remained near its original orientation, i.e., the TMV, indicating that practically no rigid body rotation has occurred. Therefore, this domain precisely locates the ancient central axis (CA) of the spreading center. This domain has a width of 6 km and probably represents the lower oceanic crust beneath the neo-volcanic zone, a zone that does not suffer significant rotational deformation (e.g., [40,41]). The width of the inferred lower crust neo-volcanic zone stands in agreement with the prediction of Gee and Meurer [34] for 6 km width of the region where magma is re-supplied into the lower crust at the Mid-Atlantic Ridge, south of Kane fracture zone. This pattern of no rotation bounds the location of the spreading axis near the Arakapas transform fault. Furthermore, this portion of the oceanic crust should be the southern continuation of the paleo-Solea axis, exposed north of the plutonic

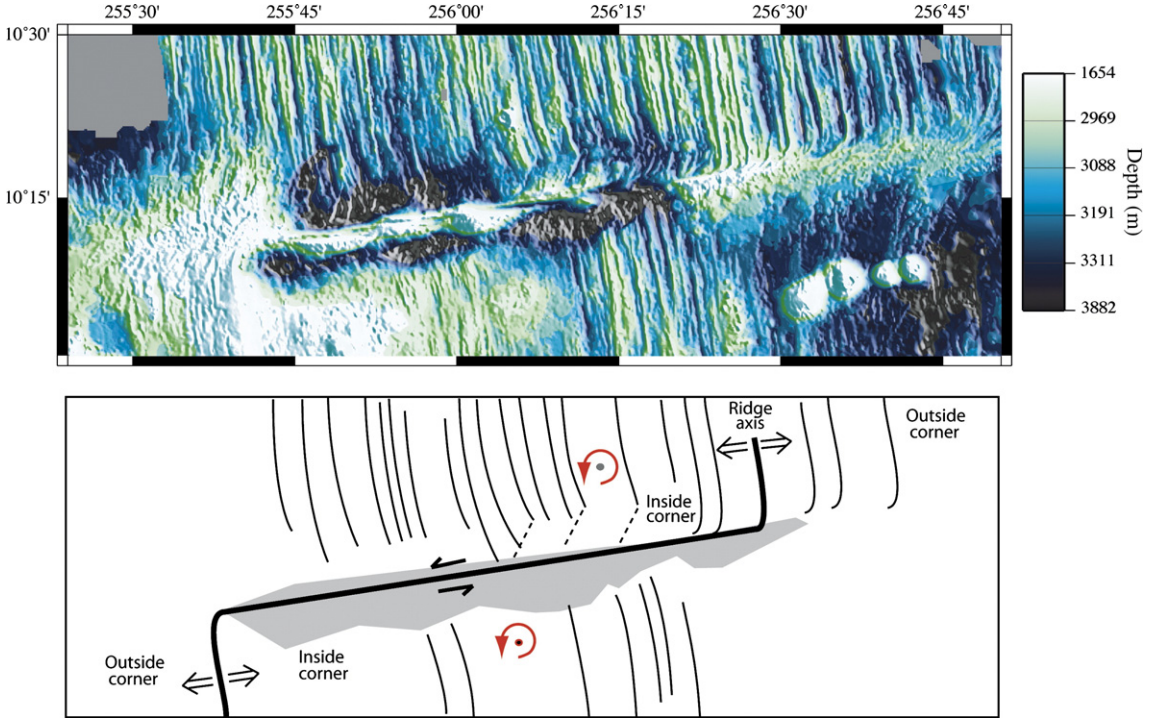

Fig. 5. Bathymetric map showing left lateral motion along the Clipperton transform fault (top, [45]), and a sketch of the main structures near this plate boundary (bottom). Note the curvature of the abyssal hills (thin lines) in the inside corners, far from the ridge axis. These J-shaped structures are the N–S inverted replica of the Troodos sheeted dikes configuration due to the opposite sense of motion on the transform faults. Shaded gray demonstrates highly deformed area, and dashed lines symbolize suspected faults.

complex, and consequently, the examination of Domains 1-3 supports an orthogonal RTI configuration (Fig. 6) and will be used in the subsequent rotational reconstruction (i.e., N–S tilt axis).

The paleo-spreading axis inferred by MacLeod et al. [20] is located more westerly than our findings from the gabbro suite (Fig. 6). This small offset seems to stem from the tilt of the upper crust rotated blocks (Fig. 8).

5.3. Lower crust versus upper crust rotation in the Troodos RTI — implications to the thermal and mechanical structure of the axial lithosphere

5.3.1. Outside corner

The OC (Domain 1) exposes gabbroic rocks that have only undergone 30–60° rotation about a horizontal axis. Moreover, the adjacent sheeted dikes have also suffered 45–90° rotation in the same sense (Figs. 4a and 7) [14].

For example, site T-23, located near Lemithou in an area where dikes have been rotated to almost horizontal positions (Fig. 7). A localized detachment fault zone, separating the dikes from the gabbroic section underlies these dikes. Hurst et al. [27] have collected paleomagnetic cores within the hanging wall, i.e., the sheeted dikes (site 5–78). Their results revealed magnetic declination of 024° and inclination of 65° (α_{95}=6.5°), suggesting that the dikes rotated ~ 65° about a subhorizontal N–S oriented axis, assuming that the dikes intruded vertically, subparallel to spreading axis, and initially acquired TMV magnetization direction. Their back-tilting procedure brought the magnetization of the dikes to the TMV and their walls to orient in a nearly vertical position. Our paleomagnetic results from the gabbro site (T-23) show SMV declination of 183° and inclination of 80.9° (α_{95}=6.8°), indicating rotation of 54° (Fig. 7). These results primarily imply that the dikes and gabbros went through a similar amount of rotation about a similar rotation axis. The localized detachment fault beneath the tilted dikes suggests that the relative small difference in the rotation between the dikes and gabbro may have occurred by decoupling along that fault.

Comparison between the gabbro suite and the sheeted dikes rotations suggests that in the OC, at least the upper part of the lower crust and above are responding to extensional stresses in the same manner. The paleomagnetic comparison also suggests that for the most part, the oceanic crust tilted as a whole, probably over a deeper yet unexposed detachment faults. This tilting might also be partly the result of an isostatic uplift linked to the partial un-roofing of the hanging wall, upper crust.

Alternatively, a possible explanation for the magnetization discrepancy may be that some of the deformation took place while the gabbros were at temperatures above T_c. In that case, no detachment between these two units is needed to explain the different rotations. However, the inference that the seismogenic zone in the oceanic crust is below 600 °C [38,39], and the appearance of detachment fault in between support our assumption that the magnetization records the entire rigid body rotation.

Our results agree with recent paleomagnetic results from the Mid-Atlantic Ridge that indicate lower crustal rotations of ~ 60° [6]. Yet, Kelemen et al. [6] have showed similar rotations on both sides of the spreading

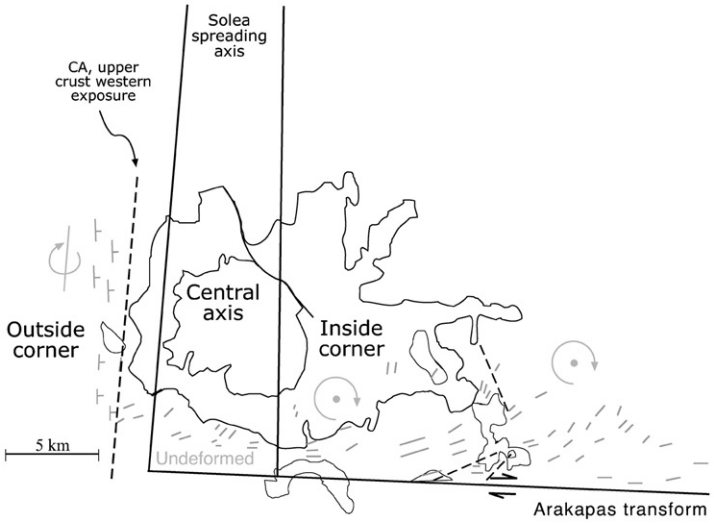

Fig. 6. Schematic representation of the Solea orthogonal RTI configuration at the lower crust. Gray arrows refer to the deformation state of the lower crust. Dashed line represents the western exposure of the central spreading axis within the upper crust [20].

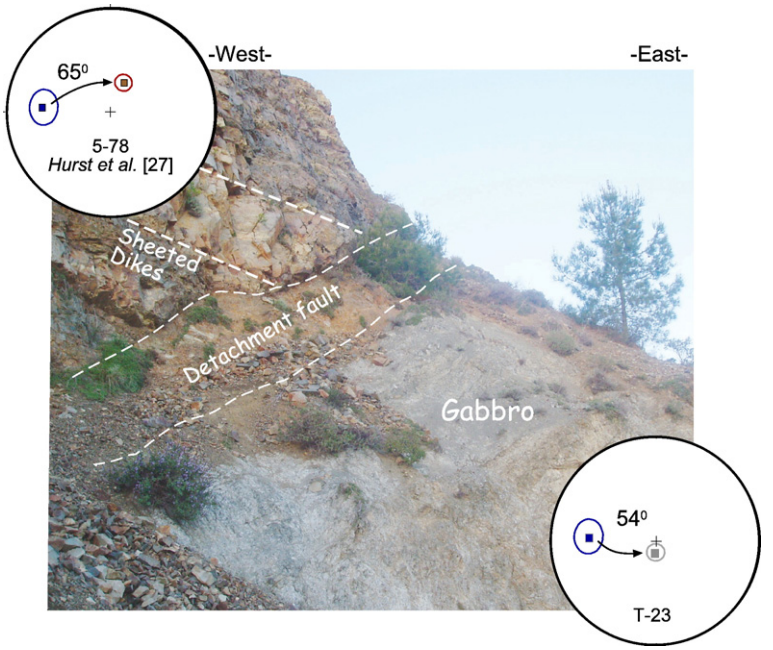

Fig. 7. Outcrop of the outside corner detachment fault near Lemithou. Lower hemisphere projections of the paleomagnetic results are shown adjacent to the fault that detaches horizontal sheeted dikes from gabbros. Results from the gabbro outcrop, site T-23, are shown in the lower right corner. Results from the sheeted dikes are shown in the upper left corner, modified from Hurst et al. [27], site 5–78. Shallow westerly ellipses represent TMV. Arrows and degrees represent sense and degree of finite rotation. Dashed white lines demarcate the detachment fault and the sheeted dikes planes.

axis, whereas here we show different rotational behavior for the IC and OC. We speculate that the reasons for the apparent conflict are different mechanical strength of the transform faults and different magmatic evolution processes for the two spreading environments.

5.3.2. Central axis

The lower crust along the inferred paleo-spreading axis has not undergone significant rotation. However, the sheeted dikes immediately adjacent to Domain 2 (exposed to the south) are rotated about a vertical axis. This abrupt rotational difference between the sheeted dikes and the gabbro in domain 2, suggests decoupling between the brittle sheeted dikes of the upper crust and the ductile axial lower crust. This observation implies brittle–ductile transition elevated to shallower depths at the fossil-spreading axis relatively to the IC and OC terrains (Fig. 8).

Deepening of the brittle–ductile transition away from the spreading axis is likely to suggest enhancement in

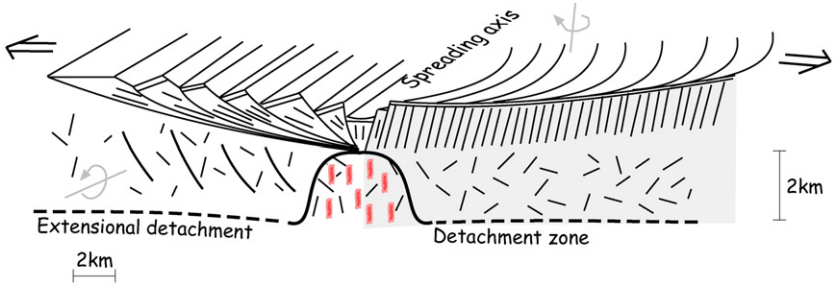

Fig. 8. Ridge-perpendicular cross section of the Solea spreading axis demonstrating the evolution of the Troodos upper oceanic lithosphere along the orthogonal RTI. Dikes within the outside corner rotate about a horizontal axis. Dikes within the inside corner rotate about a vertical axis. The lithosphere cools and thickens as it moves away from the spreading axis, consequently, the detachment faults migrate downward below the level of the measured gabbro outcrops. Most of the deformation occurs in this stage. Shaded gray demonstrates the face of the Arakapas transform fault, thick black lines demonstrate detachment faults.

the lithosphere thickness that is probably caused by cooling of the oceanic lithosphere as it spreads away from the ridge axis (Fig. 8).

According to the ATLB model of Agar and Klitgord [24], the characteristic magnetization vectors should have been significantly rotated upward (Fig. 2). However, Domain 2 demonstrates magnetization directions quite similar to the TMV with little upward rotation, suggesting that the ATLB model is likely to overestimate the antithetic rotations and the mechanical differences within the Troodos crust.

5.3.3. Inside corner

The IC exposes gabbroic rocks that experienced clockwise rotation up to 60° about a vertical axis. On the other hand, the sheeted dikes show 60–80° rotation at the same sense (Fig. 4b) [20,22]. This means that in the IC terrain the lower crust deforms at the same sense as the upper crust, but the amount of rotation is smaller. The difference in the amount of rotation is probably due to the decoupling at early stage of accretion as identified in the CA terrain, where the sheeted dikes were decoupled from the axial gabbros. This decoupling separated the two layers allowing a difference of 5–20° in the cumulative vertical axis rotation (Fig. 4b). The rotation discrepancy remains constant at various distances from the spreading axis suggesting that most of the deformation within the crust occurs together, probably over a deeper detachment zone relatively far from the spreading center (Fig. 8). The asymmetric deformational behavior between the outside and inside corners is clear in the gabbro and sheeted dikes layers, taking an opening velocity of 20–70 mm/yr [42], at least for the first 300,000 years after accretion.

Progressive clockwise rotation is observed for the mean magnetic vectors from 17 sites in Domains 2–3. These vectors exhibit a gradual increase in the amount of rotation about a vertical axis with increasing distance from the Solea axis (Fig. 4b). This deformational pattern further suggests that this area was accreted along the Solea spreading axis. Increasingly clockwise rotation together with increasing distance from the spreading axis implies a dextral nature of the Arakapas transform fault with a simple shear mechanism. The scattering in the paleomagnetic vectors is typical for the Troodos gabbro as already found by Abelson et al. [25] for a single site of a layer gabbro as well as in the eastern part of the gabbro suite. The scattering is likely to reflect secular variations in the geomagnetic field during the magnetic quiet zone.

5.4. Implications for the study of the oceanic crust

Our data demonstrate that the magnetization of the lower oceanic crust can be used to precisely locate the region where magma is supplied into the lower crust, and consequently to locate paleo-spreading axes in ophiolites. Based on our results, tectonic analysis of abandoned structures in present-day oceanic crust is possible using the magnetization of gabbros. Our results indicate that the lower crust plays a central role in the accommodation of extension within the oceanic crust. Spatial understanding of lower crustal deformation near RTIs opens new opportunities for mechanical and kinematical modeling.

6. Summary

New paleomagnetic mapping from the Troodos gabbro suite indicates that the magnetization of the lower oceanic crust can be used to constrain rigid body rotation of the oceanic crust. We have identified three structural domains describing the structure of the fossil ridge-transform intersection as well as the fossil axial-volcanic-zone based on the paleomagnetic results. Domain 1 represents the lower crust OC with a block rotation about horizontal axis. Domain 2 represents the lower crust in the fossil spreading axis with negligible rigid body rotation, decoupled from the rotated sheeted dike complex of the upper crust. Minor rotations in this domain suggest the finding of the lower crust within the axial-volcanic-zone and elevated brittle–ductile transition. Domain 3 embodies the deformation expected for the IC, where block rotation is about a vertical axis. The inferred Solea axis through the gabbro indicates an orthogonal RTI configuration.

The finding of high structural level of decoupling between the gabbro and the sheeted dikes at the fossil spreading axis, versus the coupling between these two layers in the IC and OC terrains, may indicate deepening of the brittle–ductile transition away from the spreading axis. This enhancement in the lithosphere thickness is probably caused by cooling of the oceanic lithosphere as it spreads away from the ridge axis.

Acknowledgments

We would like to thank Jeff Gee and Lisa Tauxe for generously providing many helpful comments on the manuscripts. We also thank two anonymous reviewers for their constructive comments, and Gideon Baer and Oded Navon for their useful discussion during an early stage of the research. We thank Eli Ram for the field

assistance. Data for Fig. 5 were obtained from Marine Geoscience, Data Management System, http://www.marine-geo.org and prepared using GMT [43].

References

[1] K.C. Macdonald, B.P. Luyendyk, Investigation of faulting and abyssal hill formation on the flanks of the East Pacific Rise (21-Degrees-N) using Alvin, Mar. Geophys. Res. 7 (1985) 515–535.

[2] R.J. Varga, J.A. Karson, J.S. Gee, Paleomagnetic constraints on deformation models for uppermost oceanic crust exposed at the Hess Deep Rift: implications for axial processes at the East Pacific Rise, J. Geophys. Res. 109 (2004), doi:10.1029/2003JB002486.

[3] L.J. Sonder, R.A. Pockalny, Anomalously rotated abyssal hills along active transforms: distributed deformation of oceanic lithosphere, Geology 27 (1999) 1003–1006.

[4] K.A. Kriner, R.A. Pockalny, R.L. Larson, Bathymetric gradients of lineated abyssal hills: inferring seafloor spreading vectors and a new model for hills formed at ultra-fast rates, Earth Planet. Sci. Lett. 242 (2006) 98–110.

[5] S. Allerton, M.A. Tivey, Magnetic polarity structure of the lower oceanic crust, Geophys. Res. Lett. 28 (2001) 423–426.

[6] P.B. Kelemen, E. Kikawa, D.J. Miller, et al., Shipboard Scientific Party, Leg 209 summary (2004) 1–139.

[7] J.A. Karson, R.M. Lawrence, Tectonic window into gabbroic rocks of the middle oceanic crust in the MARK area near sites 921–924, Proc. Ocean Drill. Program Sci. Results 153 (1997) 61–76.

[8] H.J.B. Dick, H. Schouten, P.S. Mayer, D.G. Gallo, H. Bergh, R. Tyce, P. Patriat, K.T.M. Johnson, J. Snow, A.T. Fisher, Tectonic evolution of the Atlantis II fracture zone, Proc. Ocean Drill. Program Sci. Results 118 (1991) 359–398.

[9] R.J. Varga, E.M. Moores, Spreading structure of the Troodos ophiolite, Cyprus, Geology 13 (1985) 846–850.

[10] E.M. Moores, F.J. Vine, Troodos Massif, Cyprus and other ophiolites as oceanic crust — evaluation and implications, Philos. Trans. R. Soc. London Ser. 268A (1971) 443–466.

[11] S.B. Mukasa, J.N. Ludden, Uranium–lead isotopic ages of plagiogranites from the Troodos ophiolite, Cyprus, and Their Tectonic Significance, Geology 15 (1987) 825–828.

[12] W.B. Harland, R.L. Armstrong, A.V. Cox, L.E. Craig, A.G. Smith, D.G. Smith, Geological Time Scale, Cambridge University Press, Cambridge, 1990.

[13] J.A. Pearce, Basalt geochemistry used to investigate past tectonic environments on Cyprus, Tectonophysics 25 (1975) 41–67.

[14] S.D. Hurst, E.M. Moores, R.J. Varga, Structural and geophysical expression of the Solea graben, Troodos ophiolite, Cyprus, Tectonics 13 (1994) 139–156.

[15] A. Robertson, C. Xenophontos, Development of concepts concerning the Troodos ophiolite and adjacent units in Cyprus, in: H.M. Prichard, T. Alabaster, N.B.W. Harris, C.R. Neary (Eds.), Magmatic Processes and Plate Tectonics, Geol. Soc. Spec. Publ., vol. 76, 1993, pp. 85–119.

[16] C.J. Macleod, A.H.F. Robertson, S. Allerton, P. Browning, I.G. Gass, R.N. Taylor, F.J. Vine, C. Xenophontos, Tectonic evolution of the Troodos ophiolite within the Tethyan framework — comment, Tectonics 11 (1992) 910–915.

[17] K.O. Simonian, I.G. Gass, Arakapas fault belt, Cyprus — fossil transform fault, Geol. Soc. Am. Bull. 89 (1978) 1220–1230.

[18] C.J. Macleod, B.J. Murton, On the sense of slip of the Southern Troodos transform–fault zone, Cyprus, Geology 23 (1995) 257–260.

[19] A. Morris, K.M. Creer, A.H.F. Robertson, Paleomagnetic evidence for clockwise rotations related to dextral shear along the southern Troodos transform-fault, Cyprus, Earth Planet. Sci. Lett. 99 (1990) 250–262.

[20] C.J. Macleod, S. Allerton, I.G. Gass, C. Xenophontos, Structure of a fossil ridge-transform intersection in the Troodos ophiolite, Nature 348 (1990) 717–720.

[21] S. Allerton, F.J. Vine, Deformation styles adjacent to transform faults: evidence from the Troodos ophiolite, Cyprus, in: L.M. Parson, B.J. Murton, P. Browning (Eds.), Ophiolites and their modern oceanic analogues, Geol. Soc. Spec. Publ., vol. 60, 1992, pp. 251–261.

[22] N. Bonhommet, P. Roperch, F. Calza, Paleomagnetic arguments for block rotations along the Arakapas Fault (Cyprus), Geology 16 (1988) 422–425.

[23] S. Allerton, Distortions, rotations and crustal thinning at ridge transform intersections, Nature 340 (1989) 626–628.

[24] S.M. Agar, K.D. Klitgord, A mechanism for decoupling within the oceanic lithosphere revealed in the Troodos ophiolite, Nature 374 (1995) 232–238.

[25] M. Abelson, G. Baer, A. Agnon, Fossil ridge–transform intersection in the Troodos ophiolite: new perspectives from rock magnetism in the gabbro suite and fracture mechanics analysis, Geochem. Geophys. Geosyst. 3 (2002), doi:10.1029/2001GC000245.

[26] T.M.M. Clube, A.H.F. Robertson, The paleorotation of the Troodos microplate, Cyprus, in the late Mesozoic–early Cenozoic Plate tectonic framework of the Eastern Mediterranean, Surv. Geophys. 8 (1986) 375–437.

[27] S.D. Hurst, K.L. Verosub, E.M. Moores, Paleomagnetic constraints on the formation of the Solea graben, Troodos ophiolite, Cyprus, Tectonophysics 208 (1992) 431–445.

[28] R.J. Varga, J.S. Gee, H. Staudigel, L. Tauxe, Dike surface lineations as magma flow indicators within the sheeted dike complex of the Troodos ophiolite, Cyprus, J. Geophys. Res. 103 (1998) 5241–5256.

[29] T.M.M. Clube, K.M. Creer, A.H.F. Robertson, Paleorotation of the Troodos microplate, Cyprus, Nature 317 (1985) 522–525.

[30] M. Abelson, G. Baer, A. Agnon, Evidence from gabbro of the Troodos ophiolite for lateral magma transport along a slow-spreading mid-ocean ridge, Nature 409 (2001) 72–75.

[31] G. Yaouancq, C.J. MacLeod, Petrofabric investigation of gabbros from the Oman Ophiolite: comparison between AMS and rock fabric, Mar. Geophys. Res. 21 (2000) 289–305.

[32] D.G. Rao, K.S. Krishna, Magnetic rock properties of the gabbros from the ODP Drill Hole 1105A of the Atlantis Bank, Southwest Indian Ridge, Proc. Indian Academy Sci. 111 (2002) 467–481.

[33] J.E. Pariso, P.R. Kelso, C. Richter, Paleomagnetism and rock magnetic properties of gabbro from Hole 894G, Hess Deep, Proc. Ocean Drill. Program Sci. Results 147 (1996) 373–381.

[34] J.S. Gee, W.P. Meurer, Slow cooling of middle and lower oceanic crust inferred from multicomponent magnetizations of gabbroic rocks from the Mid-Atlantic Ridge south of the Kane fracture zone (MARK) area, J. Geophys. Res. 107 (2002), doi:10.1029/2000JB000062.

[35] J. Malpas, Crustal accretionary processes in the Troodos ophiolite, Cyprus: evidence from field mapping and deep crustal drilling, in: J. Malpas, E.M. Moores, A. Panayiotou, C. Xenophontos (Eds.), Troodos 1987 on Ophiolites and Oceanic

Analogues, Geol. Surv. Dept., Ministry of Agriculture and Natural Resources of Cyprus, Nicosia, 1990, pp. 65–74.
[36] J.L. Kirschvink, The least-squares line and plane and the analysis of paleomagnetic data, Geophys. J. Roy. Astr. Soc. 62 (1980) 699–718.
[37] R.A. Fisher, Dispersion on a sphere, Proc. Roy. Soc. Lond. 217 (1953) 295–305.
[38] R.E. Abercrombie, G. Ekstrom, Earthquake slip on oceanic transform faults, Nature 410 (2001) 74–77.
[39] A.B. Watts, S. Zhong, Observations of flexure and the rheology of oceanic lithosphere, Geophys. J. Int. 142 (2000) 855–875.
[40] B.E. Tucholke, J. Lin, A geological model for the structure of ridge segments in slow-spreading ocean crust, J. Geophys. Res. 99 (1994) 11937–11958.
[41] S.C. Solomon, D.R. Toomey, The structure of midocean ridges, Ann. Rev. Earth Planet. Sci. 20 (1992) 329–364.
[42] C. Small, Global systematics of mid-ocean ridge morphology, in: R.W. Buck, P.T. Delaney, J.A. Karson, Y. Lagabrielle (Eds.), Faulting and Magmatism at Mid-Ocean Ridges, American Geophys. Union, Washington DC, 1998, pp. 1–26.
[43] P. Wessel, W.H.F. Smith, New version of the generic mapping tools released, EOS Trans. AGU 76 (1995) 329.
[44] Mineral Resources Map of Cyprus, Geol. Surv. Dep., Cyprus, Nicosia, 1982.
[45] K.C. Macdonald, P.J. Fox, S. Miller, S. Carbotte, M.H. Edwards, M. Eisen, D.J. Fornari, L. Perram, R. Pockalny, D. Scheirer, S. Tighe, C. Weil, D. Wilson, The East Pacific Rise and its flanks 8–18-degrees N — history of segmentation, propagation and spreading direction based on Seamarc-Ii and sea beam studies, Mar. Geophys. Res. 14 (1992) 299–344.
[46] C.H. Jones, User-driven integrated software lives: “Paleomag” paleomagnetics analysis on the Macintosh, Comp. Geos. 28 (2002) 1145–1151.